Photothermal Activation of Metal-Organic Frameworks Using a UV-Vis Light Source

Jordi Espín,[†] Luis Garzón-Tovar,[†] Arnau Carné-Sánchez,[†] Inhar Imaz,*[†] and Daniel Maspoch*[†‡]

[†]Catalan Institute of Nanoscience and Nanotechnology (ICN2), CSIC and The Barcelona Institute of Science and Technology, Campus UAB, Bellaterra, 08193 Barcelona, Spain

[‡]ICREA, Pg. Lluís Companys 23, 08010 Barcelona, Spain

ABSTRACT: Metal-Organic Frameworks (MOFs) usually require meticulous removal of the solvent molecules to unlock their potential porosity. Herein we report a novel one-step method for activating MOFs based on the photothermal effect induced by directly irradiating them with a UV-Vis lamp. The localized light-to-heat conversion produced in the MOF crystals upon irradiation enables a very fast solvent removal, thereby significantly reducing the activation time to as low as 30 min and suppressing the need for time-consuming solvent-exchange procedures and vacuum conditions. This approach is successful for a broad range of MOFs, including HKUST-1, UiO-66-NH_2, ZIF-67, CPO-27-M (M = Zn, Ni, and Mg), Fe-MIL-101-NH_2, and IRMOF-3, all of which exhibit adsorption bands in the light emission range. In addition, we anticipate that this photothermal activation can also be used to activate covalent-organic frameworks (COFs)

Keywords: Metal-organic framework, photothermal effect, activation, UV-Vis light, permanent porosity.

INTRODUCTION

Metal-organic frameworks (MOFs) are a class of porous crystalline materials built from the coordination of organic linkers and metal ions or clusters.[1-3] One of the main features of these materials is their high and tuneable porosity, which makes them good candidates for multiple applications, including gas storage and separation,[4, 5] catalysis,[6] sensing[7] and drug delivery,[8] among many others. However, a prerequisite before using MOFs in any of these applications is their activation or, in other words, the removal of all guest molecules located in their pores. These molecules can be either bound to the metal ions or residual from the synthesis solvent. The most common activation process currently entails a first step of solvent exchange, in which the solvents employed in the MOF synthesis and located in the pores are replaced by more volatile ones, followed by thermal evacuation of the solvent molecules by applying heat and/or vacuum. In other cases, in which this process damages the crystalline integrity of MOFs, milder alternative processes such as supercritical CO_2 drying, freeze drying and chemical treatment have proved useful.[9] However, most of these activation methods consist of multiple steps, require expensive equipment and/or suffer from extensive use of solvents and time. Thus, while many efforts have been devoted to optimize MOF syntheses in terms of cost, safety and environmental criteria, there is a lack of alternative one-step activation protocols that can be applied to as-synthesized MOFs.

Light-to-heat conversion (also known as the photothermal effect) has significant potential in evaporation processes due to the local nature of the heat generated, thereby minimizing heat diffusion and energy loss. This principle has already been employed in water evaporation devices by using inorganic nanoparticles,[10-12] polymers[13] and carbon based materials[14] as light-induced heaters. In MOFs, light has been exploited to trigger gas release[15-18] and in catalytic processes.[19-21] _ENREF_19 Herein, we report that this principle can be applied to activate as-synthesized MOFs in a single-step —suppressing any solvent-exchange procedure— by showing that, when irradiated with high-intensity UV-Vis light, MOFs exhibiting adsorption bands in the range 300-650 nm (light emission range) reach high temperatures (above 120 °C) within minutes, and that this localized heat can efficiently remove the trapped and coordinated solvent molecules from the MOF structure, thereby generating activated MOFs in unprecedentedly short times at atmospheric pressure (Figure 1a). We have demonstrated this concept by activating several MOFs covering the most representative subfamilies, including HKUST-1, UiO-66, UiO-66-NH_2, ZIF-8, ZIF-67, CPO-27-M (M = Zn, Ni, and Mg), Fe-MIL-101-NH_2, and IRMOF-3. In all cases, the activated MOFs retain their crystallinity and show BET surface areas (S_{BET}) comparable to the highest reported values. Moreover, a covalent-organic framework (COF-TAPB-BTCA) was activated using this method, suggesting that this concept could be extended to other COFs.

EXPERIMENTAL SECTION

Materials and instrumentation

Reagents and solvents were purchased from Sigma Aldrich and Fisher Scientific, respectively, and used without further purification. Deionized water was obtained using a Milli-Q system (18.2 MΩ cm). X-ray powder diffraction (XRPD) patterns were collected using an X'Pert PRO MPDP analytical diffractometer (Panalytical) at 45 kV and 40 mA with a CuKα radiation source (λ =

1.5419 Å). Nitrogen adsorption measurements were carried out at 77 K using an Autosorb-IQ-AG analyser (Quantachrome Instruments). Solid-state UV-Vis spectra were recorded using a Cary 4000 spectrophotometer (Agilent Technologies) in the wavelength range 200-800 nm, previously preparing KBr pellets of the samples. The UV-Vis high-intensity spot lamp without filter (300-650 nm) was a Bluepoint 4 Ecocure (Hönle UV Technology), and the infrared camera was a PI 450 (Optris), working in a temperature range of 0-250 °C. Data were obtained using the PI Connect software.

Synthetic procedures

Synthesis of HKUST-1. In a typical synthesis,[22] a solution of 2 g (8.5 mmol) of $Cu(NO_3)_2 \cdot 2.5H_2O$ and 1.20 g (5.5 mmol) of 1,3,5-benzenetricarboxylic acid (BTC) in 50 mL of a mixture of dimethylformamide (DMF), ethanol and water (1:1:1) was spray-dried in a B-290 Mini Spray-dryer (BÜCHI Labortechnik) at a feed rate of 4.5 $mL \cdot min^{-1}$, a flow rate of 336 $mL \cdot min^{-1}$ and an inlet temperature of 180 °C, using a spray-cap with a 0.5 mm-diameter hole. After 12 min, 2.13 g of blue powder was collected. This powder was washed several times with 40 mL of methanol and recovered by centrifugation. The final product was air-dried.

Synthesis of UiO-66. In a typical synthesis,[23] 0.68 g (2.9 mmol) of $ZrCl_4$ in 15 mL of a mixture of DMF and water (5.48:1 v/v) was added to a solution of 0.48 g (2.9 mmol) of benzene-1,4-dicarboxylic acid (BDC) in 15 mL of DMF. The resulting mixture was heated at 120 °C under stirring for 2 h. The solid obtained was collected by centrifugation, washed twice with 20 mL of DMF and twice with 20 mL of absolute ethanol, and finally air-dried overnight.

Synthesis of UiO-66-NH_2. In a typical synthesis,[23] 3.5 mL of 37% HCl was added to a solution of 1.17 g (5 mmol) of $ZrCl_4$ and 0.91 g (5 mmol) of 2-aminoterephthalic acid (NH_2-BDC) in 50 mL of DMF. The resulting mixture was heated at 120 °C under stirring for 2 h. The solid obtained was collected by centrifugation, washed twice with 20 mL of DMF and twice with 20 mL of absolute ethanol, and finally air-dried overnight.

Synthesis of ZIF-8. In a typical synthesis,[24] a solution of 0.30 g (1.4 mmol) of $Zn(OAc)_2 \cdot 2H_2O$ in 5 mL of deionized (DI) water was added to a solution of 1.12 g (13.6 mmol) of 2-methylimidazole (2-MIM) in 5 mL of DI water. The resulting mixture was homogenised by stirring for a few seconds, then the mixture was left to stand at room temperature for 6 h. White crystals were recovered by centrifugation, washed three times with 20 mL of methanol, and finally air-dried.

Synthesis of ZIF-67. In a typical synthesis,[24] a solution of 0.60 g (2.4 mmol) of $Co(OAc)_2 \cdot 4H_2O$ in 5 mL of DI water was added to a solution of 2.24 g (27.3 mmol) of 2-MIM in 5 mL of DI water. The resulting mixture was homogenised by stirring for a few seconds, then the mixture was left to stand for 2 h at room temperature. Purple crystals were collected by centrifugation, washed three times with 20 mL of methanol, and finally air-dried.

Synthesis of CPO-27-Zn. In a typical synthesis,[25] a solution of 0.36 g (1.8 mmol) of 2,5-dihydroxyterephthalic acid (DHTA) in 5.0 mL of sodium hydroxide solution (0.29 g, 7.3 mmol) was added to a solution of 0.79 g (3.6 mmol) of $Zn(OAc)_2 \cdot 2H_2O$ in 5.0 mL of DI water. The resulting yellow suspension was stirred for 60 min at room temperature. The product was collected by centrifugation, washed twice with DI water (30 mL) and twice with 30 mL of methanol, and finally air-dried overnight.

Synthesis of CPO-27-Ni. In a typical synthesis,[25] a solution of 0.09 g (0.5 mmol) of DHTA in 10.0 mL of sodium hydroxide solution (0.07 g, 1.8 mmol) was added to a solution of 0.22 g (0.88 mmol) of $Ni(OAc)_2 \cdot 4H_2O$ in 10.0 mL of DI water. The resulting green solution was stirred at room temperature for 24 h. The product was collected by centrifugation, washed three times with 30 mL of DI water and three times with 30 mL of methanol, and finally air-dried overnight.

Synthesis of CPO-27-Mg. In a typical synthesis,[25] a solution of 0.18 g (0.9 mmol) of DHTA in 5.0 mL of sodium hydroxide solution (0.15 g, 3.8 mmol) was added to a solution of 0.48 g (2.2 mmol) of $Mg(OAc)_2 \cdot 4H_2O$ in 5.0 mL of DI water. The resulting green suspension was stirred for 6 h at room temperature. The product was collected by centrifugation, washed three times with 30 mL of DI water and three times with 30 mL of methanol, and finally air-dried overnight.

Synthesis of Fe-MIL-101-NH_2. The synthesis was adapted from reported procedures.[26] Thus, 0.68 g (2.5 mmol) of $FeCl_3 \cdot 6H_2O$ in 7.5 mL of DMF was added to a solution of 0.225 g (1.2 mmol) of NH_2-BDC in 7.5 mL of DMF and the resulting mixture heated at 120 °C for 24 h. The solid obtained was collected by centrifugation, then washed three times with 20 mL of DMF and twice with 20 mL of absolute ethanol. The resulting powder was air-dried overnight. To eliminate most of the free NH_2-BDC, the product was dispersed in DMF at 110 °C under stirring for 8 h and precipitated by centrifugation. This process was repeated three times.

Synthesis of IRMOF-3. The synthesis was adapted from reported procedures.[27] Thus, 1.20 g (4 mmol) of $Zn(NO_3)_2 \cdot 6H_2O$ and 0.30 g (1.6 mmol) of NH_2-BDC were dissolved in 40 mL of DMF. The solution was divided into 8 scintillation vials and heated at 100 °C for 24 h in an oven. Crystals were harvested from the bottom of these vial, then washed twice with 10 mL of DMF and 10 mL of chloroform. Dried crystals were kept under an argon atmosphere.

Synthesis of COF-TAPB-BTCA. COF-TAPB-BTCA was synthesized following a previously reported method.[28] In a

typical synthesis, 0.03 g (0.2 mmol) of 1,3,5-benzenetricarbaldehyde (BTCA) in 12.5 mL of acetone and 2.5 mL of acetic acid was added to a solution of 0.06 g (0.2 mmol) of 1,3,5-tris-(4-aminophenyl)benzene (TAPB) in 12.5 mL of acetone. The resulting mixture was stirring for 1 h. The obtained yellow solid was collected by centrifugation, washed two times with 20 mL of acetone and two times with 20 mL of THF. After that, the solid was dispersed in a mixture of 1,4-dioxane and mesitylene (9:1 v/v), adding 1.75 mL of water and 2.6 mL of acetic acid under continuous stirring at room temperature. The resulting mixture was heated at 80 °C under stirring for 8 days. The obtained solid was collected by centrifugation at 9000 rpm for 4 min, washed three times with 10 mL of toluene, and finally air-dried.

Light guide to sample distance effect. It is known that the irradiance of a lamp changes depending on the proximity of the irradiated body. To assess the light intensity received per surface unit of MOF in our activation experiments, the detector of a power meter (Newport 1918-C) was systematically placed at different distances (3, 4, 5, 6,7, 8 and 9 cm), the UV-Vis lamp turned on at 100 % power and the irradiance measured for each distance. Figure S1 shows the irradiance ($mW \cdot cm^{-2}$) as a function of the inverse squared distance (cm^{-2}), which follows the inverse-square law ($I \alpha 1 / r^2$).[29, 30]

Photothermal effect characterization. 100 mg of each MOF was spread on a quartz slide to form a thin round layer with the largest possible surface area (diameter of between 2 and 3.5 cm) at a distance of 7 cm from the light guide, which corresponds to an irradiance of 500 $mW \cdot cm^{-2}$. The infrared camera was placed next to the irradiation setup focusing on the MOF sample, and video recording was started just before the UV-Vis lamp was set to 100 % intensity. The recorded video allowed the temperature change to be plotted against time. The blank experiment involved irradiating the quartz slide holder alone and proved that there was no change in temperature.

UV-Vis activation procedure. In a typical UV-Vis activation experiment, 100 mg of each MOF was first placed in a three-neck round-bottomed flask. The light guide was then introduced via the central neck and placed at a distance of 7 cm from the MOF sample. In some cases, the separation between the MOF and the light guide was reduced to 5 cm and 3 cm, corresponding to irradiances of 900 and 2650 $mW \cdot cm^{-2}$, respectively. The neck was then wrapped with parafilm. Both side necks were capped with a septum and a needle. One of these necks was used as the gas inlet attached to the argon tube, whereas the other served as the gas purge. Once the argon flow had been adjusted (8 Normal Liter Per Minute ($NL \cdot min^{-1}$)), the UV-Vis lamp was turned on, irradiating the MOF sample for the desired time at 100 % intensity (Figure S2). When the exposure time was finished, the light guide was removed from the flask, which was rapidly capped with a septum, kept under argon and subsequently introduced into the glovebox, where the powder was weighed in the gas sorption cell under an argon atmosphere. The MOF sample was then transferred from the glovebox to the gas sorption equipment, where the N_2 isotherm was measured for further BET surface area (S_{BET}) calculation.

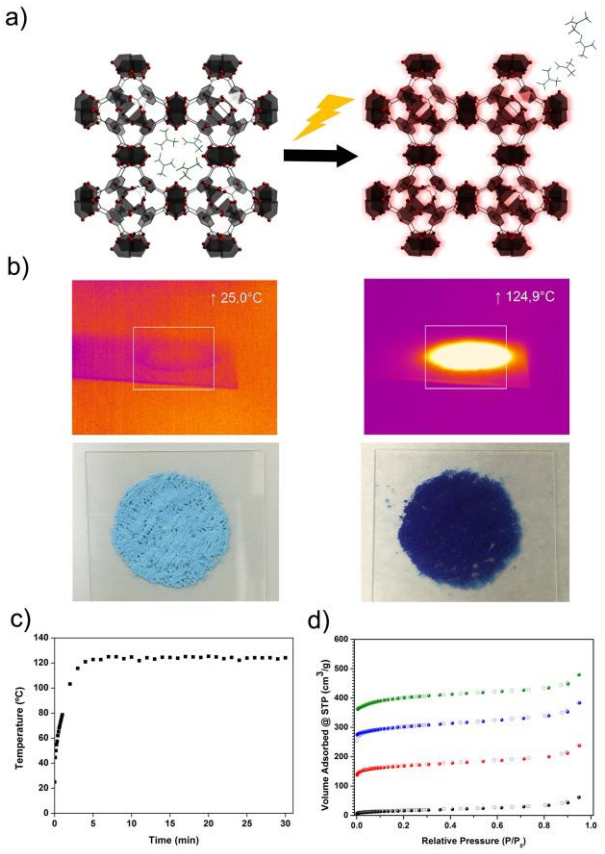

Figure 1. a) Schematic representation of the photothermal activation of MOFs. b) IR camera pictures (top) of HKUST-1 before (left) and during UV-Vis irradiation (right). Photographs of HKUST-1 powder (bottom) before (left) and after (right) irradiation. c) Temperature evolution as a function of time for HKUST-1 irradiated at a distance of 7 cm. d) N2 adsorption isotherms for HKUST-1 after 30 min of heat treatment (red) and after photothermal activation for 5 min (blue) and 30 min (green), in comparison to the as-synthesized sample (black).

RESULTS AND DISCUSSION

Photothermal activation of HKUST-1. HKUST-1 was chosen to benchmark the UV-Vis activation protocol due to its well-standardized activation process. Indeed, HKUST-1 is usually activated using several solvent-exchange steps (*e.g.* with dichloromethane or methanol) followed by a thermal treatment (from 80 to 170 °C) under vacuum, thus resulting in S_{BET} values ranging from 1450 to 1800 $m^2 \cdot g^{-1}$ when fully activated.[31, 32]

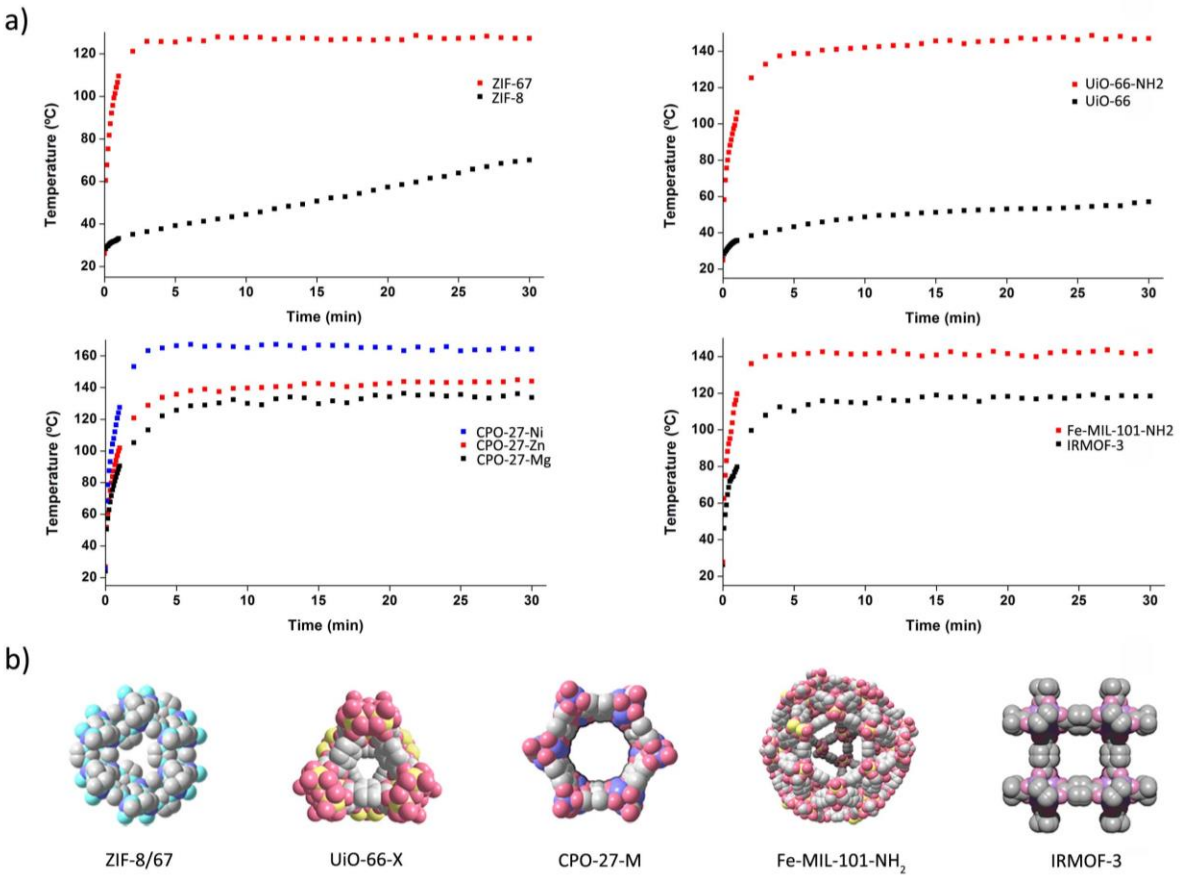

Figure 2. a) Temperature evolution as a function of time for all studied MOFs when irradiated at a distance of 7 cm. b) Representation of the crystalline structure of the studied MOFs.

Our experiment started with an evaluation of the photothermal effect on a sample of as-synthesized HKUST-1 by monitoring the temperature change with irradiation time (Figure 1). It was found that HKUST-1 was immediately heated when exposed to UV-Vis light, reaching a plateau at 120 °C after irradiation for 4-5 min (Figure 1b and c, Video S1). The strong photothermal effect could be rationalized by analysing the solid state UV-Vis spectrum of HKUST-1, which showed a broad absorption band centred at 720 nm attributed to the d-d transitions of the Cu(II) in the paddle wheel,[33] which falls with the wavelength used in the irradiation experiments (Figures S3-5). The contribution of this absorption band was further studied by irradiating HKUST-1 in a wavelength range of 320-390 nm (UV) and of 390-500 nm (Visible). As expected, in both cases, lower temperatures (40 °C and 60 °C, respectively) were reached, demonstrating that light of wavelengths close to the maximum absorption band in the visible range mainly contributes to the photothermal effect (Figure S6). It is noteworthy that the colour of the HKUST-1 powder changed from sky blue to deep purple after the irradiation experiments (Figure 1b). This colour change was a first clear evidence of the removal of the solvent molecules coordinated to the Cu(II) paddle-wheel clusters.

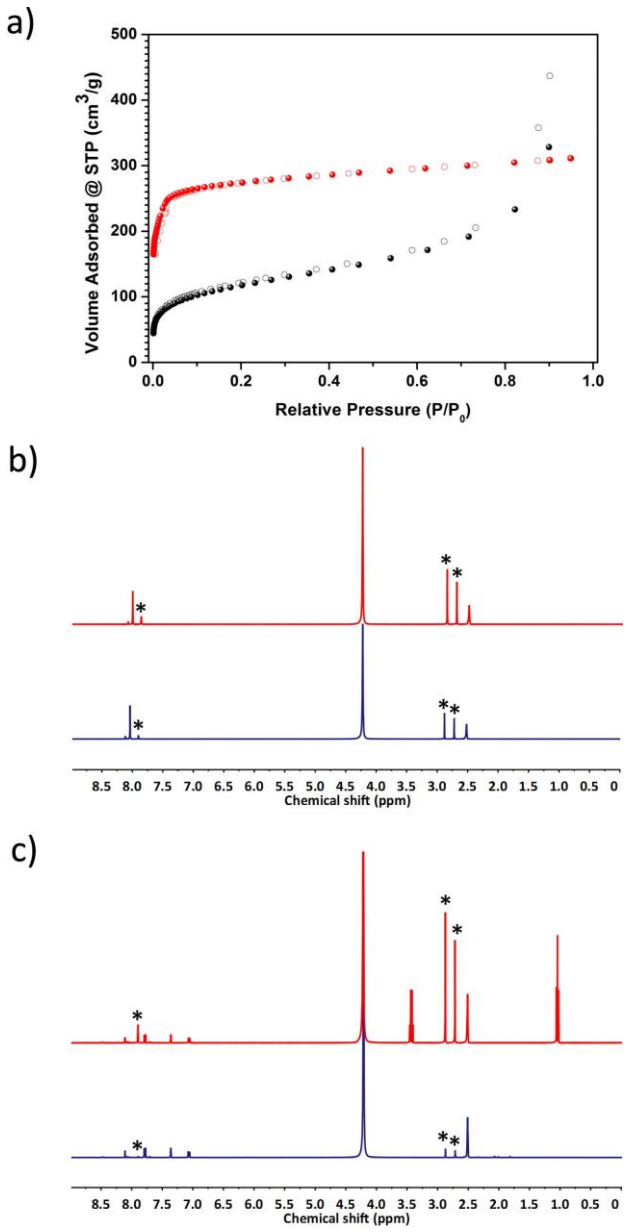

Figure 3. a) N_2 adsorption isotherms for UiO-66 (black) and UiO-66-NH_2 (red) after photothermal activation. b) ^1H NMR spectra of as-synthesized UiO-66 (red) and after photothermal activation (blue). c) ^1H NMR spectra of as-synthesized UiO-66-NH_2 (red) and after photothermal activation (blue). DMF peaks are highlighted with an asterisk (*).

To assess the efficiency of the photothermal activation, we then measured the XRPD and S_{BET} for HKUST-1 samples irradiated for 5 and 30 min without any further treatment (Figure 1d). XRPD indicated that both irradiated samples retain the crystallinity of the initial HKUST-1 MOF (Figure S7). Remarkably, the HKUST-1 irradiated for only 5 min showed an S_{BET} of 1209 $m^2 \cdot g^{-1}$ (Figure S8), and increasing the irradiation time increased this value further. Indeed, after irradiation for 30 min the S_{BET} value had increased to 1583 $m^2 \cdot g^{-1}$ (Figure S9). These results confirm that the photothermal effect in HKUST-1 is sufficiently intense to evacuate both trapped and coordinated solvent molecules from the framework. We hypothesize that the high efficiency of the photothermal activation method to evacuate solvent molecules is due to the localized heat generation, which minimizes heat loss. In order to further confirm this hypothesis, HKUST-1 was heated to 120 °C for 30 min but using an external heating source such as a heating mantle. In this case, the S_{BET} of the thermally treated sample was significantly lower (S_{BET} = 655 $m^2 \cdot g^{-1}$, Figure S10), thus highlighting the benefits of UV-Vis induced localized heating on solvent removal from the HKUST-1 framework.

An important factor that can influence the photothermal activation of MOFs is the MOF-to-light guide distance. To evaluate this parameter, we studied the photothermal activation of HKUST-1 by reducing this distance to 5 and 3 cm, thus meaning that the irradiance increased to 900 and 2650 $mW \cdot cm^{-2}$, respectively. As expected, shorter distances meant that HKUST-1 reached a higher temperature (Figure S11). When irradiated for 5 min, HKUST-1 reached a maximum of 187 °C (distance = 5 cm) and above 250 °C (distance = 3 cm). These different heating conditions were critical for HKUST-1 activation. Indeed, while HKUST-1 irradiated at 3 cm was found to be amorphous and non-porous, the sample irradiated at 5 cm retained its crystallinity and showed an S_{BET} of 1819 $m^2 \cdot g^{-1}$ (Figures S12-13). This result is remarkable since it demonstrates that HKUST-1 can be activated in only 5 min, and that the MOF-to-light guide distance is a parameter that can be tuned to optimize the photothermal activation of MOFs (*vide infra*).

Versatility of the photothermal activation method. To demonstrate the scope of this activation method beyond HKUST-1, we used it to study the activation of a series of MOFs representing the major subfamilies of porous MOFs. The MOFs studied comprised UiO-66, UiO-66-NH_2, ZIF-8, ZIF-67, CPO-27-M (where M is Zn(II), Ni(II), and Mg(II)), Fe-MIL-101-NH_2, and IRMOF-3. Figure 2 shows the photothermal response of each of these MOFs as a function of time. Two different behaviours can be seen from this figure. Thus, MOFs that do not exhibit an absorption band in the range 300-650 nm (light emission range; Figures S17,27) showed a mild temperature increase after irradiation for 30 min. For example, UiO-66 and ZIF-8 were heated to 57 and 70 °C, respectively. In contrast, MOFs that show adsorption bands in this range exhibited a much higher photothermal effect (Figures S18, 28 36, 41, 48). The temperatures reached for each of these MOFs irradiated for 30 min were as follows: IRMOF-3 (119 °C), ZIF-67 (127 °C), CPO-27-Mg (136 °C), Fe-MIL-101-NH_2 (143 °C), CPO-27-Zn (145 °C), UiO-66-NH_2 (149 °C), and CPO-27-Ni (167 °C). Moreover, as in HKUST-1, each of these latter

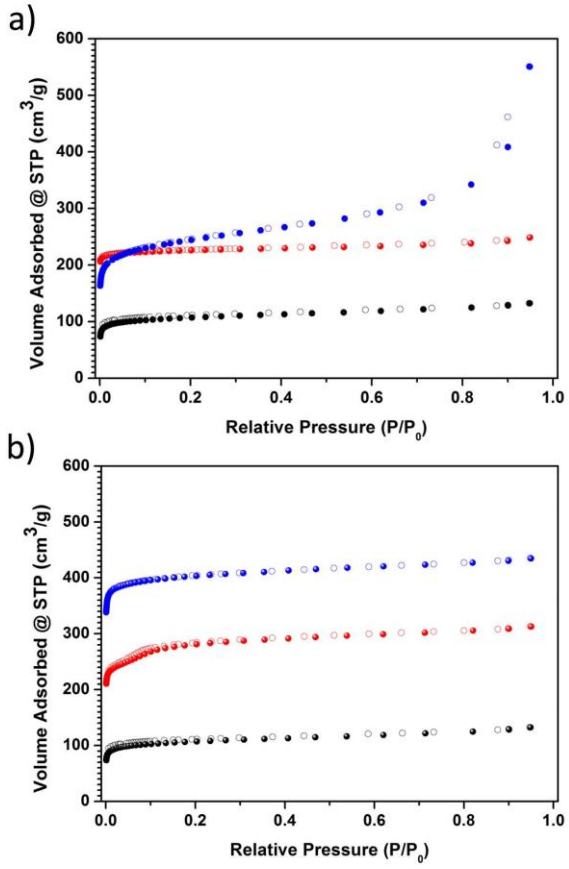

Figure 4. (a) N_2 adsorption isotherms of CPO-27-Mg (black), - Zn (red) and -Ni (blue) after irradiated at 500 mW·cm^{-2}. (b) N_2 adsorption isotherms of CPO-27-Mg after irradiated at 500 (black), 900 (red) and 2650 mW·cm^{-2} (blue).

Table 1. Summary of the main parameters of the photothermally activated materials.

Material	Photohermal Temperature (ºC)	η (%)*	S_{BET} (m^2 g^{-1})		Residual solvent (%)**
			This work	Reported	
HKUST-1	125	33.6	1583	1740[31]	5.1[a]
UiO-66	57	5.0	424	1580[35]	11.2[b]
UiO-66-NH_2	149	59.3	1098	1200[35]	3.4[b]
ZIF-8	60	0.3	1130	1079[36]	-[c]
ZIF-67	127	50.0	1666	1319[38]	-[c]
CPO-27-Zn	145	23.8	932	1154[25]	1.7[d]
CPO-27-Ni	167	93.6	922	1351[25]	0.4[d]
CPO-27-Mg	136	21.6	1630	1603[25]	2.0[d]
Fe-MIL-101-NH_2	143	86.6	1506	2436[39]	1.8[a]
IRMOF-3	119	25.8	2556	2850[40]	3.6[b]
COF-TAPB-BTCA	136	55.4	1185	1120[28]	3.0[e]

*Calculated as explained in the SI.

**Calculated from the residual [a]DMF and EtOH, [b]DMF, [d]MeOH, and eacetone. [c]Note that H_2O could not be determined by NMR.

MOFs reached their maximum temperature after irradiation for only 4-5 min.

Once the photothermal effect of the selected MOFs had been assessed, we studied their activation using the UV-Vis light source. The photothermal activation of UiO-66 and UiO-66-NH_2 was initially compared due to the differences in their photothermal behaviour but similarities in their structure. In addition, it is known that the activation of UiO-66 analogues is quite challenging because of the presence of DMF molecules in the pores, which cannot be completely removed unless a long solvent-exchange process is carried out. Accordingly, both MOFs were irradiated for 30 min, with no further treatment, and their XRPD patterns and S_{BET} subsequently measured. Again, XRPD indicated that both irradiated samples retained the crystallinity of the initial UiO-66 type MOFs (Figures S19, 20). However, the N_2 adsorption isotherms showed a clear difference in their activation (Figure 3a). Thus, while the irradiated UiO-66-NH_2 showed an S_{BET} of 1098 $m^2 \cdot g^{-1}$ (close to the highest reported value;[34, 35] Figure S22), the irradiated UiO-66 showed a much lower S_{BET} of 424 $m^2 \cdot g^{-1}$, in accordance with its weaker photothermal effect (Figure 2 and Figure S21). This difference was further studied by first digesting the as-synthesized and irradiated UiO-66 and UiO-66-NH_2 samples, and then analysing the resulting solutions by ^{1}H NMR spectroscopy (Figure 3b,c and Figures S23-S24). We then calculated the percentage of DMF molecules removed from both frameworks during the activation process by comparison of the integration of one peak at 7.90 ppm corresponding to DMF and those at 8.02 and 7.78 ppm corresponding to BDC and NH_2-BDC, respectively. From these data, it was clear that photothermal activation was more efficient at evacuating the DMF molecules from the UiO-66-NH_2 framework (94 % of the initial DMF molecules were evacuated) than from the UiO-66 framework (only 55 % were evacuated). This fact correlates well with the higher temperature and photothermal transduction efficiency (η) reached by UiO-66-NH_2 (149 °C and 59.3 %) in comparison to that reached for UiO-66 (57 °C and 5.0 %) when irradiated for 30 min (Table 1 and Section S10).

A similar but less pronounced trend was also found when both ZIF-8 and ZIF-67 were irradiated. The S_{BET} for the irradiated ZIF-8 was 1130 $m^2 \cdot g^{-1}$ (calculated from the second step of the isotherm between 0.01 and 0.2 P/P_0; Figure S31), which is lower than typical reported values ($S_{BET} \approx$ 1400-1500 $m^2 \cdot g^{-1}$).[36, 37] In contrast, the photothermally activated ZIF-67 exhibited an S_{BET} of 1666

$m^2 \cdot g^{-1}$ (calculated from the second step of the isotherm between 0.01-0.2 P/P_0; Figure S32), which is comparable to the highest reported values.[38] In this case, however, ZIF-8 showed a significant degree of activation despite its mild photothermal effect (Figure 2). We attribute this effect to the efficiency of the localized heat together with the lack of open metal sites in the structure and the non-high boiling point solvents used in the synthesis (water) and washing (methanol) steps, which significantly reduces the energy required to remove occluded solvent molecules (Figures S33-S34).

The efficient photothermal activation was further proven for Fe-MIL-101-NH_2 and IRMOF-3 (Figures S35-S44). In both cases, the irradiated MOFs exhibited good S_{BET} values of 1506 and 2556 $m^2 \cdot g^{-1}$, respectively.[39, 40] It is important to highlight here that IRMOF-3 has been reported to require supercritical CO_2 activation to achieve an optimum S_{BET} value (2850 $m^2 \cdot g^{-1}$).[40] Therefore, our activation method seems to respect less robust MOFs, most likely due to the localised and homogeneous heating produced and the lack of high vacuum conditions.

In accordance with this observation, we also tested our activation method with some CPO-27 analogues as activation of this MOF family is quite difficult due to the presence of open metal sites that strongly coordinate with water molecules.[25] Activation of these MOFs generally entails a long solvent-exchange process (from 6 to 12 days) with methanol followed by high-temperature thermal treatments (above 180 °C) under vacuum. Consequently, three members of this MOF family were activated by UV-Vis light irradiation for 30 min. In all cases, irradiated CPO-27-Zn/-Ni/-Mg retained the initial crystallinity (Figure S49-51) and showed a change in colour, which was a first indication of the removal of solvent molecules coordinated to the respective metal centres (Figure S45-47). In fact, the successful photothermal activation of CPO-27-Zn and CPO-27-Ni was accomplished with only 30 min of UV-Vis irradiation, as demonstrated by the measured S_{BET} values of 932 $m^2 \cdot g^{-1}$ for CPO-27-Zn and 922 $m^2 \cdot g^{-1}$ for CPO-27-Ni (Figure 4a, Figure S52, 53).[25]

However, these activation conditions were not found to be optimum to efficiently activate CPO-27-Mg (S_{BET} = 416 $m^2 \cdot g^{-1}$, Figure S54). In this case, photothermal activation was optimized by reducing the MOF-to-light guide distance down to 5 cm (irradiance = 900 $mW \cdot cm^{-2}$) and 3 cm (irradiance = 2650 $mW \cdot cm^{-2}$; Figure S1). Under these new conditions, CPO-27-Mg reached a temperature of 184 and 250 °C, respectively, when irradiated for 30 min. In both cases, XRPD showed that the crystallinity was maintained (Figure S55). In addition, the measured S_{BET} values confirmed a better activation process, with values of 1062 and 1630 $m^2 \cdot g^{-1}$ (the latter being comparable to the highest reported values; Figure 4b)[25] when exposed to a light power of 900 and 2650 $mW \cdot cm^{-2}$, respectively.

Finally, we opened up the possibility of using this photothermal activation method in covalent organic frameworks (COFs). To this end, a two-dimensional COF (COF-TAPB-BTCA) assembled from two trigonal building blocks, 1,3,5-benzenetricarbaldehyde (BTCA) and 1,3,5-tris-(4-aminophenyl)benzene (TAPB) (Figure S61), was irradiated at a distance of 7 cm (irradiance = 500 $mW \cdot cm^{-2}$) for 30 min, obtaining an S_{BET} value of 1185 $m^2 \cdot g^{-1}$, which is comparable to that reported in the literature (Figure S66).[28] Similar to the MOFs, this COF also reached a temperature of 136 °C after irradiation for 4-5 min.

CONCLUSIONS

In summary, we have reported that a UV-Vis lamp can be used to activate as-synthesized MOFs in a single step. MOFs with adsorptions in the UV-Vis wavelength range emitted by this lamp undergo a significant heating (120–220 °C) in 4-5 min. This localized light-to-heat conversion in the MOF crystals when irradiated enables a very fast solvent removal, thereby significantly reducing the activation time down to 30 min and supressing the need for time-consuming solvent-exchange procedures and vacuum conditions. We have found that the S_{BET} values obtained after photothermal activation for only 30 min are comparable to the highest reported values for the conventionally activated HKUST-1, ZIF-67, UiO-66-NH_2, Fe-MIL-101-NH_2, IRMOF-3 and CPO-27-M (M = Ni, Zn and Mg). Moreover, we have demonstrated that this activation method could be extended to COFs. Our findings should facilitate the integration of an activation step in processes in which MOFs/COFs are manufactured in a continuous way as well as the use of this photothermal effect in applications in which the triggered desorption of volatile species (*e.g.* water) is desired.

ASSOCIATED CONTENT

Supporting Information

The Supporting Information is available free of charge via the Internet at http://pubs.acs.org.

Lamp irradiance calibration, setup description, photographs and infrared camera pictures before and after irradiation, solid-state UV-Vis spectra, XRPD patterns, N_2 adsorption isotherms, phothermal plots, NMR spectra, photothermal transduction efficiency calculations and infrared camera video.

AUTHOR INFORMATION

Corresponding Author

*(I.I.) E-mail: inhar.imaz@icn2.cat
*(D.M.) E-mail: daniel.maspoch@icn2.cat

ORCID

Jordi Espín: 0000-0001-6381-6259

Luis Garzón Tovar: 0000-0003-0253-4041

Arnau Carné-Sánchez: 0000-0002-8569-6208

Inhar Imaz: 0000-0002-0278-1141

Daniel Maspoch: 0000-0003-1325-9161

Author Contributions

The manuscript was written through contributions of all authors. All authors have given approval to the final version of the manuscript.

Notes

The authors declare no competing financial interest.

ACKNOWLEDGMENT

This work was supported by the Spanish MINECO (projects PN MAT2015-65354-C2-1-R), the Catalan AGAUR (project 2014 SGR 80), the ERC under the EU FP7 (ERC-Co 615954), and European Union's Horizon 2020 research and innovation programme under grant agreement No 685727. It was also funded by the CERCA Programme / Generalitat de Catalunya. ICN2 acknowledges the support of the Spanish MINECO through the Severo Ochoa Centers of Excellence Program, under Grant SEV-2013-0295. J.E. acknowledges the MINECO for the FPI fellowship.

ABBREVIATIONS

XRPD, X-ray powder diffraction; UV-Vis, Ultraviolet-Visible; DI, deionized water; MOF, metal-organic framework; COF, covalent-organic framework; DMF, dimethylformamide; NMR, nuclear magnetic resonance; PTE, photothermal transduction efficiency.

REFERENCES

(1) Furukawa, H.; Ko, N.; Go, Y. B.; Aratani, N.; Choi, S. B.; Choi, E.; Yazaydin, A. Ö.; Snurr, R. Q.; O'Keeffe, M.; Kim, J.; Yaghi, O. M. Ultrahigh Porosity in Metal-Organic Frameworks. *Science*, **2010**, *329*, 424-428.

(2) Kitagawa, S.; Kitaura, R.; Noro, S.-i. Functional Porous Coordination Polymers. *Angew. Chem. Int. Ed.*, **2004**, *43*, 2334-2375.

(3) Zhou, H.-C.; Long, J. R.; Yaghi, O. M. Introduction to Metal–Organic Frameworks. *Chem. Rev.*, **2012**, *112*, 673-674.

(4) Murray, L. J.; Dinca, M.; Long, J. R. Hydrogen Storage in Metal-Organic Frameworks. *Chem. Soc. Rev.*, **2009**, *38*, 1294-1314.

(5) Makal, T. A.; Li, J.-R.; Lu, W.; Zhou, H.-C. Methane Storage in Advanced Porous Materials. *Chem. Soc. Rev.*, **2012**, *41*, 7761-7779.

(6) (a) Lee, J.; Farha, O. K.; Roberts, J.; Scheidt, K. A.; Nguyen, S. T.; Hupp, J. T. Metal-Organic Framework Materials as Catalysts. *Chem. Soc. Rev.*, **2009**, *38*, 1450-1459. (b) Jiao, L.; Wang, Y.; Jiang, H-L.; Xu, Q. Metal–Organic Frameworks as Platforms for Catalytic Applications. *Adv. Mater.*, **2017**, *DOI: 10.1002/adma.201703663.* (c) Yang, Q.; Xu, Q.; Jiang, H-L.; Metal–organic frameworks meet metal nanoparticles: synergistic effect for enhanced catalysis. *Chem. Soc. Rev.*, **2017**, *46*, 4774-4808.

(7) Kreno, L. E.; Leong, K.; Farha, O. K.; Allendorf, M.; Van Duyne, R. P.; Hupp, J. T. Metal–Organic Framework Materials as Chemical Sensors. *Chem. Rev.*, **2012**, *112*, 1105-1125.

(8) Horcajada, P.; Gref, R.; Baati, T.; Allan, P. K.; Maurin, G.; Couvreur, P.; Férey, G.; Morris, R. E.; Serre, C. Metal–Organic Frameworks in Biomedicine. *Chem. Rev.*, **2012**, *112*, 1232-1268.

(9) Mondloch, J. E.; Karagiaridi, O.; Farha, O. K.; Hupp, J. T. Activation of Metal–Organic Framework Materials. *CrystEngComm*, **2013**, *15*, 9258-9264.

(10) Neumann, O.; Urban, A. S.; Day, J.; Lal, S.; Nordlander, P.; Halas, N. J. Solar Vapor Generation Enabled by Nanoparticles. *ACS Nano*, **2013**, *7*, 42-49.

(11) Wang, Z.; Liu, Y.; Tao, P.; Shen, Q.; Yi, N.; Zhang, F.; Liu, Q.; Song, C.; Zhang, D.; Shang, W.; Deng, T. Bio-Inspired Evaporation Through Plasmonic Film of Nanoparticles at the Air–Water Interface. *Small*, **2014**, *10*, 3234-3239.

(12) Liu, Y.; Yu, S.; Feng, R.; Bernard, A.; Liu, Y.; Zhang, Y.; Duan, H.; Shang, W.; Tao, P.; Song, C.; Deng, T. A Bioinspired, Reusable, Paper-Based System for High-Performance Large-Scale Evaporation. *Adv. Mater.*, **2015**, *27*, 2768-2774.

(13) Zhang, L.; Tang, B.; Wu, J.; Li, R.; Wang, P. Hydrophobic Light-to-Heat Conversion Membranes with Self-Healing Ability for Interfacial Solar Heating. *Adv. Mater.*, **2015**, *27*, 4889-4894.

(14) Ghasemi, H.; Ni, G.; Marconnet, A. M.; Loomis, J.; Yerci, S.; Miljkovic, N.; Chen, G. Solar Steam Generation by Heat Localization. *Nat. Commun.*, **2014**, *5*, 4449.

(15) Li, H.; Hill, M. R.; Doblin, C.; Lim, S.; Hill, A. J.; Falcaro, P. Visible Light Triggered CO_2 Liberation from Silver Nanocrystals Incorporated Metal–Organic Frameworks. *Adv. Funct. Mater.*, **2016**, *26*, 4815-4821.

(16) Li, H.; Hill, M. R. Low-Energy CO_2 Release from Metal–Organic Frameworks Triggered by External Stimuli. *Acc. Chem. Res.*, **2017**, *50*, 778-786.

(17) Khaletskaya, K.; Reboul, J.; Meilikhov, M.; Nakahama, M.; Diring, S.; Tsujimoto, M.; Isoda, S.; Kim, F.; Kamei, K.-i.; Fischer, R. A.; Kitagawa, S.; Furukawa, S. Integration of Porous Coordination Polymers and Gold Nanorods into Core–Shell Mesoscopic Composites toward Light-Induced Molecular Release. *J. Am. Chem. Soc.*, **2013**, *135*, 10998-11005.

(18) Diring, S.; Carne-Sanchez, A.; Zhang, J.; Ikemura, S.; Kim, C.; Inaba, H.; Kitagawa, S.; Furukawa, S. Light Responsive Metal-Organic Frameworks as Controllable CO-Releasing Cell Culture Substrates. *Chem. Sci.*, **2017**, *8*, 2381-2386.

(19) Yang, Q.; Xu, Q.; Yu, S.-H.; Jiang, H.-L. Pd Nanocubes@ZIF-8: Integration of Plasmon-Driven Photothermal Conversion with a Metal–Organic Framework for Efficient and Selective Catalysis. *Angew. Chem. Int. Ed.*, **2016**, *55*, 3685-3689.

(20) Wang, F.; Huang, Y.; Chai, Z.; Zeng, M.; Li, Q.; Wang, Y.; Xu, D. Photothermal-enhanced Catalysis in Core-shell Plasmonic Hierarchical Cu_7S_4 Microsphere@Zeolitic Imidazole Framework-8. *Chem. Sci.*, **2016**, *7*, 6887-6893.

(21) Chen, Y.-Z.; Wang, Z. U.; Wang, H.; Lu, J.; Yu, S.-H.; Jiang, H.-L. Singlet Oxygen-Engaged Selective Photo-Oxidation over Pt Nanocrystals/Porphyrinic MOF: The Roles of Photothermal Effect and Pt Electronic State. *J. Am. Chem. Soc.*, **2017**, *139*, 2035-2044.

(22) Carné-Sánchez, A.; Imaz, I.; Cano-Sarabia, M.; Maspoch, D. A Spray-Drying Strategy for Synthesis of Nanoscale Metal–Organic Frameworks and their Assembly into Hollow Superstructures. *Nat. Chem.*, **2013**, *5*, 203-211.

(23) Ragon, F.; Horcajada, P.; Chevreau, H.; Hwang, Y. K.; Lee, U. H.; Miller, S. R.; Devic, T.; Chang, J.-S.; Serre, C. In Situ Energy-Dispersive X-ray Diffraction for the Synthesis Optimization and Scale-up of the Porous Zirconium Terephthalate UiO-66 *Inorg. Chem.*, **2014**, *53*, 2491-2500.

(24) Avci, C.; Ariñez-Soriano, J.; Carné-Sánchez, A.; Guillerm, V.; Carbonell, C.; Imaz, I.; Maspoch, D. Post-Synthetic Anisotropic Wet-Chemical Etching of Colloidal Sodalite ZIF Crystals. *Angew. Chem. Int. Ed.*, **2015**, *54*, 14417-14421.

(25) Garzon-Tovar, L.; Carne-Sanchez, A.; Carbonell, C.; Imaz, I.; Maspoch, D. Optimised Room Temperature, Water-Based Synthesis of CPO-27-M Metal-Organic Frameworks with High Space-Time Yields. *J. Mater. Chem. A*, **2015**, *3*, 20819-20826.

(26) Bauer, S.; Serre, C.; Devic, T.; Horcajada, P.; Marrot, J.; Férey, G.; Stock, N. High-Throughput Assisted Rationalization of the Formation of Metal Organic Frameworks in the Iron(III) Aminoterephthalate Solvothermal System. *Inorg. Chem.*, **2008**, *47*, 7568-7576.

(27) Tanabe, K. K.; Wang, Z.; Cohen, S. M. Systematic Functionalization of a Metal−Organic Framework via a Postsynthetic Modification Approach. *J. Am. Chem. Soc.*, **2008**, *130*, 8508-8517.

(28) Rodríguez-San-Miguel, D.; Yazdi, A.; Guillerm, V.; Pérez-Carvajal, J.; Puntes, V.; Maspoch, D.; Zamora, F. Confining Functional Nanoparticles into Colloidal Imine-Based COF Spheres by a Sequential Encapsulation–Crystallization Method. *Chem. - Eur. J.*, **2017**, *23*, 8623-8627.

(29) Born, M.; Wolf, E. Principles of Optics: Electromagnetic Theory of Propagation, Interference and Diffraction of Light, Cambridge University Press, Cambridge, **1999**.

(30) McCluney, W. R. Introduction to Radiometry and Photometry, Second Edition, Artech House Publishers, Boston/London, **2014**.

(31) Kim, H. K.; Yun, W. S.; Kim, M. B.; Kim, J. Y.; Bae, Y. S.; Lee, J.; Jeong, N. C. A Chemical Route to Activation of Open Metal Sites in the Copper-Based Metal–Organic Framework Materials HKUST-1 and Cu-MOF-2. *J. Am. Chem. Soc*., **2015**, *137*, 10009-10015.

(32) Song, X.; Jeong, S.; Kim, D.; Lah, M. S. Transmetalations in Two Metal-Organic Frameworks with Different Framework Flexibilities: Kinetics and Core-Shell Heterostructure. *CrystEngComm*, **2012**, *14*, 5753-5756.

(33) Prestipino, C.; Regli, L.; Vitillo, J. G.; Bonino, F.; Damin, A.; Lamberti, C.; Zecchina, A.; Solari, P. L.; Kongshaug, K. O.; Bordiga, S. Local Structure of Framework Cu(II) in HKUST-1 Metallorganic Framework: Spectroscopic Characterization upon Activation and Interaction with Adsorbates. *Chem. Mater*., **2006**, *18*, 1337-1346.

(34) Hu, Z.; Zhao, D. De facto Methodologies Toward the Synthesis and Scale-up Production of UiO-66-Type Metal-Organic Frameworks and Membrane Materials. *Dalton Trans*., **2015**, *44*, 19018-19040.

(35) Katz, M. J.; Brown, Z. J.; Colon, Y. J.; Siu, P. W.; Scheidt, K. A.; Snurr, R. Q.; Hupp, J. T.; Farha, O. K. A Facile Synthesis of UiO-66, UiO-67 and their Derivatives. *Chem. Commun*., **2013**, *49*, 9449-9451.

(36) Pan, Y.; Liu, Y.; Zeng, G.; Zhao, L.; Lai, Z. Rapid Synthesis of Zeolitic Imidazolate Framework-8 (ZIF-8) Nanocrystals in an Aqueous System. *Chem. Commun*., **2011**, *47*, 2071-2073.

(37) Lee, Y.-R.; Jang, M.-S.; Cho, H.-Y.; Kwon, H.-J.; Kim, S.; Ahn, W.-S. ZIF-8: A Comparison of Synthesis Methods. *Chem. Eng. J*., **2015**, *271*, 276-280.

(38) Shi, Q.; Chen, Z.; Song, Z.; Li, J.; Dong, J. Synthesis of ZIF-8 and ZIF-67 by Steam-Assisted Conversion and an Investigation of Their Tribological Behaviors. *Angew. Chem. Int. Ed*., **2011**, *50*, 672-675.

(39) Savonnet, M.; Kockrick, E.; Camarata, A.; Bazer-Bachi, D.; Bats, N.; Lecocq, V.; Pinel, C.; Farrusseng, D. Combinatorial Synthesis of Metal-Organic Frameworks Libraries by Click-Chemistry. *New J. Chem*., **2011**, *35*, 1892-1897.

(40) Nelson, A. P.; Farha, O. K.; Mulfort, K. L; Hupp, J. T. Supercritical Processing as a Route to High Internal Surface Areas and Permanent Microporosity in Metal−Organic Framework Materials. *J. Am. Chem. Soc*., **2009**, *131*, 458-460.

Table of Contents